Seismic performance of the St. George of the Latins church: Lessons learned from studying masonry ruins

Paulo B. Lourenço[1, *], *Alejandro Trujillo*[2], *Nuno Mendes*[3], *Luís F. Ramos*[4]

[1, *] Corresponding author. Professor, ISISE, Department of Civil Engineering, University of Minho, Azurém, P-4800-058 Guimarães, Portugal. Phone: +351 253 510 209, fax: +351 253 510 217, email: pbl@civil.uminho.pt

[2] MSc Student, ISISE, Department of Civil Engineering, University of Minho, Azurém, P-4800-058 Guimarães, Portugal. Email: alejotrurivas@gmail.com.

[3] PhD Student, ISISE, Department of Civil Engineering, University of Minho, Azurém, P-4800-058 Guimarães, Portugal. Email: nunomendes@civil.uminho.pt

[4] Assistant Professor, ISISE, Department of Civil Engineering, University of Minho, Azurém, P-4800-058 Guimarães, Portugal. Email: ramos@civil.uminho.pt

1 Introduction

Cyprus Island is located in the Eastern portion of the Mediterranean Sea; south of Turkey, west of Syria, Lebanon, and Israel, east of Greece, and north of Egypt. It is located at a confluence of Western Asia, Southern Europe and Northern Africa and has had periods of influence of several dynasties such as Byzantine, Lusignan, Genoese, Venetian, Ottoman and British. At the same time it has been the home of Armenian, Jewish, Nestorian, Maronite and Jacobite communities, see Walsh (2010).

The city of Famagusta, located in North-East Cyprus, has been over many centuries at the crossroads between the West and the East, and has played a pivotal role between the Christian and Islamic Worlds. The heritage treasures of this city combine medieval Christian churches and some impressive city walls, among other treasures. Famagusta, once known as the richest city in the world, is now threatened by earthquakes, abandonment and neglect. Due to the severe state of deterioration, it was recently placed on the 2008 World Monuments Watch List of 100 Most Endangered Sites by the World Monument Fund.

Cyprus is also located among the Alpine-Himalaya belt, which is the second most intensive seismic zone of the Earth, where the earthquakes represent about 15% of the world seismic activity. Its seismicity is attributed to the "Cyprus Arc" which is the tectonic boundary between the African and Eurasian plates. The subduction of the African Plate under the Eurasian Plate creates many earthquakes along the "Cyprus Arc" and several active faults inside the island have shown that earthquakes also occur along them (Unit of Environmental Studies, 2004).

Cyprus was stroke by strong earthquakes in the past, which destroyed and damaged towns such as Salamis (today's Famagusta) and the capital city Nicosia.

Sixteen earthquakes with intensities of VIII (on modified Mercalli scale) or higher occurred between years 26 B.C. and 1900 A.D., and two of them had big impact in Salamis (today's Famagusta) and destroyed the whole town; one occurred in 76 A.D. and the other occurred in 332 A.D. In 1896 more accurate data started to be collected when seismological stations started to operate on neighboring countries and on 1984 a seismological station was placed in Cyprus. During the period 1896-2004 more than 400 earthquakes had epicenters on Cyprus and the surrounding region, with 14 of those causing severe damages as well as victims (Unit of Environmental Studies, 2004). Two earthquakes caused damage in Famagusta since 1896: one on February 18th, 1924 with a magnitude of 6.0 that caused small damage and another on January 20th, 1941 with a magnitude 5.9 that caused severe damage.

According to the Seismic Hazard Map of Cyprus, CYS EN 1998-1:2004 (2007), the maximum peak ground acceleration (PGA) on rock for the south and west region of the island, where Famagusta is included, is about 0.25g. This value is the highest within the whole territory compared with the minimum PGA of 0.15g, which occurs in the north and center regions. Famagusta is located over Terrace deposits which are mainly formed by Calcarenites, sands and gravels, increasing the seismic demand to about 0.35g, when compared to areas that are covered with rock (Unit of Environmental Studies, 2004).

This work addresses the seismic safety of the remainings of St. George of the Latins Church, in Famagusta, including an historical survey, inspection and diagnosis.. Limit analysis of collapse mechanisms was used for a first safety assessment. Afterwards, a numerical model was prepared using finite elements and updated using dynamic identification results. The updated model was subjected to non-linear static (pushover) analysis in different directions (global and principal) using two lateral load

patterns: proportional to the mass and proportional to the mode shape of the structure in the applicable direction. The results of the pushover analyses were then compared with the limit analysis results. Non-linear dynamic analyses with time integration were also carried out, allowing a comparison between the different structural analysis techniques. One relevant contribution of the paper is the application of limit analysis collapse mechanisms to masonry remainings based on observed damage and their subsequent validation by advanced non-linear analysis of a model prepared according the Finite Element Method (FEM). It is stressed that all proposed failure mechanisms have been made before making any structural analysis.

2 Famagusta Church Remainings

From the 16th century on, Ottoman occupation of Famagusta led the city to an inevitable decline. Four and a half centuries of neglect combined with exposure to hard environmental conditions and natural phenomena, such as earthquakes, plague and flooding, left the city almost ruined by the time the British arrived in 1878 (Walsh, 2010); the historical sites and treasures of the city were completely destroyed. Despite the ambitious British' plan for restoration of Famagusta, there were only a few works carried out and the British gave priority to new prospects that were opened for trading (Municipality of Famagusta, 2009).

After the Second World War, a new era started in Famagusta, its population increased significantly and the city expanded. The inhabitants start to build their houses again and the sea font started to be filled with hotels, which was a first re-birth for the city in intellectual and economical terms. The city was again taken apart during 1974, when the Turkish troops entered to the north part of the Island and took control of

Famagusta. Hence their cultural heritage buildings have been neglected for over three decades.

According to Walsh (2007) the sandstone which is the construction material of almost all the historic monuments in Famagusta (around 200) is highly deteriorated, and the collapse of domes, arches and ribbed vaults will be inevitable if no action is taken. In order to contribute to better understand this abandoned heritage, three churches were selected for inspection as indicated in Figure 1. The churches show no evident signs of structural distress for gravitational loading, despite the need of some urgent actions for preventing injuries to visitors. Giving the earthquake hazard of the area, seismic vulnerability studies are obviously needed.

The Church of St. George of the Latins is in a ruinous state of preservation. The church still preserves its northern half, the lower section of the apse and a part of its south side, enough evidence to demonstrate that this building is an impressive example of Gothic architecture with excellent masonry, compact proportions and rich stone carving decoration. The church is dated to the end of the 13th century and it is a single-aisled building with four groin vaults which are supported by a grouping of three thin columns located in the north and south walls.

The church has some impressive gargoyles depicting human figures and winged dragons. A small conch adorned with richly decorated pediments is formed in the church's apse and was probably used to receive a sculpture. Figure 2a indicates that the present condition of the church seems not to differ significantly from the condition around 1940. Severe deterioration of the stones is reported in drawings from 1882 and several stones have been replaced in the conservation works around 1940, see Figure 2b. The present condition is characterized by, see Figure 3 and Figure 4: (a) lack of cleaning / possible misuse of the sacristy; (b) severe stone deterioration; (c) loose stone

elements, which must be consolidated or removed; (d) highly corroded reinforced concrete lintel in main door; (e) inefficient buttresses due to stone deterioration; (f) a crack / rotation of the tower, possibly due to a previous earthquake / foundation problems.

Conservation works are strongly recommended, with immediate action required in order to protect the life of visitors (Figure 3c center and right). Additional works recommended in the medium term are: (a) remove reinforced concrete lintel in main door; (b) consolidate stone shown in Figure 3c left); (c) close the open room (sacristy) with a new door. A full conservation project is needed involving at least: (a) deeper historical investigation; (b) stone replacement, stone consolidation, use of repair mortars; (c) societal involvement in the protection of the heritage / surveillance measure.

3 In situ inspection

Besides the visual inspection addressed above, also sonic testing and dynamic identification testing were carried out. Dynamic identification was made for the three churches, allowing to identify a minimum of twelve modes, see Lourenço and Ramos (2008) for details. Here, only the results for the Church of St. George of the Latins are shown.

3.1 Modal identification

Modal identification or dynamic identification analysis is a procedure that combines vibration testing techniques and analytical methods to determine modal (natural) parameters of structures. The modal parameters are frequencies, mode shapes, and damping coefficients. In other words, modal identification analysis is a diagnosis tool

used to understand how a structure responds dynamically and to calibrate the computational model of a structure.

To estimate the dynamic parameters, output-only modal identifications techniques are widely applied to civil engineering structures and to historical masonry constructions in particular. In this type of identification, structures are excited with ambient (natural) vibrations, such as the wind load, traffic or even the human induced vibrations. In this way, the excitation is considered a white noise signal (stationary Gaussian stochastic process) and only the structural response is measured with highly sensitive sensors. Once the dynamic properties of the structure are known, a numerical model (typically a Finite Element Model) can be built to simulate the structure. The mechanical properties of the numerical model should be tuned by a process called Finite Element Model Updating. This method updates the mass, stiffness and damping of the numerical model in a way that the numerical parameters (frequencies, mode shapes) are close to the experimental ones.

Three accelerometers with 10 V/g sensitivity, able to measure 0.07 mg (g the gravity acceleration), were used to measure accelerations. The sensors were connected to a laptop by a data acquisition system with 24 bit resolution with a USB cable connection. All the measurements were carried out using the natural vibration of the structures. Long periods of measurements were recorded (10 minutes), with a sampling rate of 200 points per second (200 Hz). For data processing, Stochastic Subspace Identification (SSI) methods were used (Peeters, 2000). The SSI methods estimate accurately the modal parameters (natural frequencies, mode shapes and damping coefficients) using natural vibrations.

As long periods of recording were performed, ambient temperature and relative humidity were also measured while the dynamic tests were carried on. The influence of

environmental factors in the modal parameters is well known, e.g. Ramos et al. (2010b). Figure 5 presents the variation of the environmental effects during the testing hours. The ambient temperature increased from 22 to 28ºC, while the relative air humidity decreased from 61 to 47%. The variations occurred linearly and slowly. As there are no significant changes in the environmental effects, it is expected that these parameters will not affect significantly the dynamic response of the structure.

In St. George of the Latins church the measurements were carried out in three points in the north façade. Mainly, the measurements were performed close to the top of three buttresses. The measuring points are indicated in Figure 6 using the letter A. Figure 7a-c shows images of the dynamic measurements and Figure 7d shows the stabilization diagram of the SSI method where 17 stable columns can be observed, corresponding to 17 natural frequencies of the structure below 20 Hz. The high number of modes estimated is not necessary to characterize the dynamic behavior of civil engineering structures and it is very difficult to calibrate a numerical model based on so many modes. Thus, only the first six modes were considered in the model updating.

The first six estimated natural frequencies and damping coefficients are given in Table 1. The natural frequencies range from 2.6 to 6.0 Hz. Rather close frequency values were found at 3.95 and 4.06 Hz, but in general the frequencies are well spaced. The standard deviation values for frequencies are very low, indicating that the estimation is accurate. Concerning the damping coefficients, higher variations were observed for the estimated values. The average damping value is equal to 0.81%. This low value is commonly found when ambient vibrations are used to excite the structures. As only three points were measured, the mode shape configurations are mainly out-of-plane and their resolution is low. Still, due to the unconstrained walls of the church ruins, out-of-plane modes are to be expected.

3.2 Sonic tests

Sonic tests are based on the propagation properties of solids elastic waves or pressure waves. The elastic wave crosses the walls in frequencies ranging from 0.4 to 10 kHz. Knowing the distance between two points in the wall and by measuring the travel time, it is possible to calculate the sonic velocity (the velocity of the elastic waves). For sonic tests, two types of sensors are used, the hammer for impacts transmission (or wave transmission) and the receiver that can be an accelerometer. The two sensors are connected to and data acquisition system (DAQ) that acquires at a high sampling rate, generally at 100.000 points per second, the measured quantities. The DAQ can be connected to a laptop to store and analyze the data. Depending on the sensors position, there are three types of sonic test: direct, semi-direct and indirect.

In the case that the geometry of a body or structure is known (e.g. the thickness of a wall or buttress), the time lag between the impact signal and the receiver signal allows estimating the sonic velocity inside the body, which are typically in the range of a few km/s for building materials. If materials with different density, voids or cracks occur inside another material, the sonic velocity decreases. If the body/structure is tested in several points, a sonic velocity map can be computed and will qualitatively indicate the constitution of the wall and/or the presence of voids and cracks, see e.g. Binda et al. (2003).

One stone block with 1.12 m length and two buttresses with 0.97 m thickness were tested. The stone block was selected to measure the sonic velocity of the sandstone used in the construction. The two buttresses, one in the north façade and one in the south façade, were chosen to evaluate their internal condition, mainly if there are internal voids or different density materials, or if repair works occurred in the recent past. Figure 8a shows the location of testing.

The tests were carried out with two accelerometers and one small hammer (not instrumented). The hammer was used to hit next to one accelerometer (the transmission sensor), while the other (the receiver) was placed in an opposite side of the stone or buttress, see Figure 8b. Due to constraints in the portable measurement equipment used, the sampling rate was equal to 25.000 Hz. Starting with the stone block, see Figure 8c, the average value for the sonic velocity of ten measurements was equal to 3033 m/s, with a Coefficient of Variation (CV) equal to 5%. Typical sonic velocities for old masonry are in the range of 350-2500 m/s and for stone are in the range of 2000-5000 m/s (Learid, 1984). In this case, the value found is in the mid-range of the possible values. As an example, for granites the following correlations are given in Vasconcelos et al. (2008) for the compressive f_c and tensile f_t strength:

$$f_t=0.701e^{(0.00052\ UPVdry)} \quad (1)$$

$$f_c=0.0407\ UPV_{dry} - 36.31 \quad (2)$$

where f_t is the tensile strength in N/mm^2, f_c is the compressive strength in N/mm^2 and UPV_{dry} is the ultrasonic pulse velocity for air dry conditions in m/s. If the formulas given are assumed to hold for the stone at Famagusta, rather high strength values are obtained for the stone: f_t = 3.39 MPa and f_c = 87.13MPa.

An array with two vertical columns (A and B) and five horizontal levels was considered (10 points per column). Figure 9a presents the tested points. The results are illustrated in Figure 9b and Table 2. The sonic velocity ranges from 1400 to 2400 m/s and the average value for column A and B is 1597 and 2249 m/s, respectively. Observing the color map for the velocities, it is possible to see that the outer points of the buttress (column B) have higher velocity than the inner points (column A). The

results indicate that the stones in the outer column were probably replaced by new ones in the recent past, while the internal part of the buttresses are in worse condition.

Concerning the south buttress, the velocity values for each point are also given in the last two columns of Table 2. In this buttress small differences were found between the velocity values. Ranging from 1400 to 2600 m/s, the average values for A and B were 1923 and 1996 m/s, respectively. The values indicate that the internal condition of the buttress is homogeneous, with similar distribution of voids. As the masonry tested has no joints or only a few joints, but without any fill, the values found for the sonic velocities are in the upper range of the values usually found.

4 Limit Analysis of Collapse Mechanisms

Heyman (1966) applied the modern formulation of limit analysis theory relaying on the rigid-perfectly plastic material model to evaluate the load capacity and failure mechanism of masonry arches, in a way very similar to what is known today as macro-elements. A limit condition will be reached if both statically and kinematically admissible collapsing mechanism can be found. When this occurs, the load is the true ultimate load, the mechanism is the true ultimate mechanism and the thrust line is the only one possible.

The use of limit analysis to analyze more complex masonry structures was much developed in Italy, Giuffé (1993), where experimental and theoretical studies carried out after important earthquakes demonstrated that the behavior of historical constructions was outside the range of the usual analysis approach (box behavior). Macro-element analysis techniques are deduced from the observation of seismic response, finding common collapsing configuration for structures with the same typology, and they were joined together in an abacus shown in PCM-DPC-MiBAC M.-A.-D. (2006). This

abacus takes into account twenty-eight different local failure modes for religious and civil buildings, mainly two-stories houses, churches and bell towers. A full discussion on the possibilities for the structural analysis on existing masonry structures (without box behavior) under seismic loading is given in Lourenço *et al.* (2011).

Following the principles abovementioned, the ultimate capacity of the structure depends on the stability of its macro-elements, which are portions of the structure bounded by potential damage patterns that can behave as a whole, following a kinematic mechanism. The method was applied to assess the seismic church of St. George of the Latins, as an example of a technique to be further extended to the remaining cultural heritage buildings in Famagusta. In the case of St. George of the Latins church, the macro-elements were defined according to the damage observed during the inspection works and the photographs of the restoration project carried out during 1940. In order to define the different macro-elements, the structure was divided in three different parts: west façade, the apse and its north façade. After defining the different macro-elements that compose the church, the most probable mechanism that characterize each macro-element were defined, see Valluzzi et al. (2004), considering two orthogonal set of axes: the usual transverse (X) and longitudinal (Y) directions of the church, hereby denoted by global axes, and the in-plan principal axes of the church remainings, hereby denoted by principal axes (set X',Y'), see Figure 8a. Only out-of-plane collapse mechanisms were defined, due to the obvious lack of confinement in the remainings. The arch effect was disregarded as well as the bending of the horizontal strips, and the macro-element was assumed as a rigid body except in its boundaries where cylindrical hinges are formed following the possible damage pattern controlled by cracks and openings.

Kinematic models provide a load coefficient c that represents the mass multiplier that activates the local failure mode and leads the macro-element to collapse, which can be approximated by $c = a / g$, with a equal to the peak ground acceleration and g equal to the acceleration of gravity.

The simplified procedure to assess the seismic response of a structure allows to compare the collapse coefficient obtained from the limit analysis of all the possible kinematic collapse mechanisms, and to select the lowest coefficient as the weakest one and the most probable to occur during a seismic event. Thus, collapse is due to a loss of equilibrium of its structural configuration instead of exceeding the ultimate strength of the material. Besides finding the load coefficient that activates the mechanism, the kinematic approach also allows to determine the amount of horizontal force that the macro-element is progressively able to bear in the post-peak, with the developing of the mechanism until total collapse, which occurs when the collapse coefficient is equal to zero and the structural element fully overturns. Hereby, it is possible to obtain the path of a specific point (reference control point), usually the center of mass of the macro-block. Such curve represents the capacity of the macro-element to bear horizontal force until the collapse and it is expressed by the collapse coefficient c plotted versus the total displacement of the control point, allowing a displacement based approach. This procedure is not shown here but was applied for each defined collapse mechanism following the recommendations of O.P.C.M. 3431 (2005), see Trujillo (2009).

4.1 West Façade Part

This façade is composed by a small portion of wall about 5.0 m long and 18.0 m high, with a small boxed tower (void inside) at the top, see Figure 10a. The tower suffered a rotation in the past due to a settlement or earthquake and the crack opening is shown in

Figure 10b. Also there is a stone deteriorated region in the lower part of the connection between north and west façades, see Figure 10c, which could be a possible sign of weakness in this connection. Despite restoration works carried out during 1940, see Figure 10d,e, with several stone replacements, stone deterioration concentrated in the lower part at the corner is still found, Figure 10d.

According to the damage patterns described, the possible collapse mechanisms were selected with overturning along two different directions. One kinematic mechanism considered is the overturning in –X direction of the macro-element shown in Figure 11a. This macro-element compromises the whole tower structure and two thirds (in height) of the west façade. The defined hinges are located in the upper part of the connection between north and west façades and one third (in height) of the façade, forming a tridimensional wedge. The other kinematic mechanism considered for this part of the structure is the overturning in –Y direction of the macro-element, with similar hinges, see Figure 11b.

4.2 The North Façade Part

This façade is composed by four large windows about 7.0 m high and three pier walls, see Figure 12a. Its lower part is completely massive, except for one door. There were several stone replacements in both sides of the walls, especially in the outer side of the wall. The buttresses show loss of stone elements and severe stone deterioration. In the upper part of the inner face, the stones are deteriorated and some of them are detached, see Figure 12b. This also occurs in some areas of the wall lower part. Some stones of the buttresses were replaced during 1940's restoration works; nevertheless their internal conditions are damaged, as shown by the sonic testing. The assumed failure mechanism for this part of the structure includes the three pier walls from the cornice to the top part

of the wall, and the assumed plastic hinges are shown in Figure 12c,d, where cracks are clearly defined (opening and sliding).

This collapse mechanism behaves as a rigid body meaning that the three piers rotate at the same time along the cornice located just below windows, see Figure 13, which is the first defined plastic hinge. The other two hinges are located in the connection between north and west façades and north façade and apse, as previously discussed.

4.3 The Apse Part

The apse of the church is composed by three windows and four pier walls, and the lower portion of the wall is mainly solid, with the exception of the door opening that connects the church with the sacristy. The apse buttresses are deteriorated and present a similar void distribution, in their external and internal portions as demonstrated by sonic testing. The visible damage in the buttresses is similar to other parts of the church, with high porosity, loss of material and severe decay. This part of the church is the only one that still has a part of the vaults, although they are deteriorated.

The first collapse mechanism includes a pier wall that overturns around the cornice located in the lower part of the windows, which is also the first hinge; the second hinge is located in the upper part of the window where the apse connects with the north façade and the third hinge is a straight axis along the vault vertex, see Figure 14a. Two different directions for the overturning were considered based on the structural configuration of the apse; one is the overturning of the macro-element in –X direction. The second collapse mechanism includes two pier walls, see Figure 14b. It is assumed that both pier walls will behave as a rigid body and they will rotate together and the lower plastic hinge will simultaneously appear; this hypothesis is based on the

constraint that vaults give to other movements. The other two plastic hinges are the following: one is located along the vault vertex; another one is located in the upper portion of the wall with a boundary at the end of the vault. The overturning of this macro-element was only analyzed in the only possible direction, Y direction. The definition of the last macro-element includes only the last pier wall, see Figure 14c. In the upper portion of the window located between this pier and the neighboring pier a first plastic hinge was defined. The other side of the pier wall is released; in the past it was connected with the south façade which collapsed. The rotation hinge is located in the lower cornice, just below the window and two different directions were considered for its overturning, global X direction and a principal X' direction.

4.4 Numerical Results

The load coefficient was calculated for all mechanisms, see Table 3. The minimum load coefficient in the X direction is 0.097 for the mechanism in the north façade, see Figure 13, and the minimum load coefficient for the Y direction is rather similar, with a value of 0.109 for the West façade, see Figure 11b. Therefore, according to the limit analysis approach the most vulnerable parts of the structure are the north and the west façades. It is also clear that the structure seismic stability is compromised as a PGA of 0.35g is recommended according to the National Annex of Eurocode 8 (CYS EN 1998-1:2004, 2007). A limit analysis of collapse mechanisms taking into account the finite compressive strength (f_c = E/500, see Section 5.2) was also carried out and a reduction of the load coefficient lower than 5% was found.

5 Finite Element Analysis

The finite element method was applied in order to study the church of St. George of the Latins in detail, aiming at further validating the limit analysis results and better

understand the behavior of this structure at collapse. Before making any analysis, a finite element model was prepared taking into consideration the measured frequencies and vibration modes.

5.1 Model Updating Using Dynamic Identification

The numerical model was prepared using the DIANA (2009) software using the geometrical information gathered from the historical documents and the geometrical survey. Shell elements according to the Mindlin-Reissner theory have been adopted, including shear deformation and assuming that the normal stress component perpendicular to the surface of the element is zero. The mesh was prepared using quadratic quadrilateral (eight nodes) and triangular elements (six nodes). Concentrated masses were added to the model to represent additional masses. In total, around 3,500 nodes, 1,100 elements and 18,000 degrees of freedom were obtained.

The structure is complex and several finite element models were initially considered, see Trujillo (2009). The variations considered in the models were: (a) the inclusion of the remaining part of the vaults in the apse vs. its replacement by additional masses; (b) the inclusion of the tower vs. their replacement by additional masses; (c) the possible inclusion of the existing cracks and damaged areas; (d) the possible presence of a weak connection between the north and the west façades. Afterwards, a comparison between the experimental results obtained from the dynamic tests and the numerical estimated data in each model was made and the model shown in Figure 15 was selected for further updating. The first models showed that the vaults in the apse and the tower behave as a rigid blocks. In order to simplify the model, only the vaults and tower masses (localized) were considered. The mass of these elements is known and was calibrated in model updating, in which the stiffness and mass distribution is taken into

account. The existing most significant damage is also included, by reducing the thickness of the walls. As an alternative, the reduction of the Young's modulus was rejected, since the main objective is to simulate the non-linear behavior of the structure. The option of reducing the thickness causes high stresses and strains , thus producing damage, which is in agreement with the expected physical behavior, while the thickness reduction does not.

It is also noted that the 2nd and 5th numerical modes in the different models considered were not similar to any of the first six mode shapes obtained in the experimental results. This is explained by the fact that in these two modes large displacements occur in the apse, which was not included in the dynamic identification tests. Therefore, the numerical 2nd and 5th mode shapes were disregarded in the processing of the measured data. Note also the small mass participation factors of the 2nd and 5th numerical modes, which is less than 10% in both directions for 2nd mode and less than 13% in both directions for 5th mode.

The dynamic behavior of a structure is highly affected by alterations of geometry, variations of the boundary conditions, mass changes and degradation of the mechanical properties of the materials, Ramos *et al.* (2010a). The model was calibrated following the procedure shown by Douglas and Reid (1982), which uses an optimization process to minimize the residuals between the experimental response and the numerical response. Here, only the frequencies were selected to be updated, with further validation of the numerical model by a comparison between the experimental and numerical mode shapes. The mode shapes could be included in the optimization process but due to the low resolution of modes and the additional complexity, they were disregarded in the optimization process.

It is also noted that better results are not necessarily obtained by increasing the number of parameters to be updated and the selected parameters to be updated were the elastic modulus of the masonry and the thickness that represents the reduction of stiffness in damaged areas of the real structure. The initial value for each variable, as well as the respective lower and upper bounds, should be based on experimental and historical data and engineering judgment, so that consistent results can be obtained. After the optimization the final values of all elastic parameters are given in Table 4. The deformed shapes for the first four numerical modes selected are shown in Figure 16. The results in terms of frequencies and mode shapes are shown in Table 5, as well as their comparison with experimental data in terms of average frequency estimation and Model Assurance Criterion (MAC) values. The obtained averages of the error in frequency estimation are very low (below 5%). The MAC values have a different distribution: for the 1st mode, the MAC is very good because it is higher than 90%, for the 6th mode the MAC value is acceptable because is near 80%. The MAC values for the 3rd and 4th modes are low, but can be considered acceptable in the context of a heavily damaged and discontinuous structure.

5.2 Non-Linear Static (Pushover) Analysis

Non-linear static analysis with horizontal forces adopted to represent the seismic action, also known as pushover analysis, is an alternative method of analysis to estimate the seismic response of a structure. In this analysis the structure is pushed with lateral forces distributed over the height of the building. The analysis is carried out under conditions of constant gravity loads and monotonically increasing horizontal loads that should have at least two distributions: (1) A uniform pattern based on lateral forces that are proportional to the mass regardless of their height distribution in the structure; (2) a

modal pattern proportional to lateral forces consistent with the lateral force distribution determined in the modal response analysis (EN 1998-1, 2004). Here, the first mode in each global direction with the highest mass participation factor was selected.

Pushover analysis can be applied in order to verify the structural performance of existing buildings by means of the verification of base shear ratios and the estimation of expected plastic mechanism with its damage distribution. In Mendes and Lourenço (2010), it is shown that comparable results can be found in terms of load capacity between pushover analysis and dynamic time integration analysis for masonry buildings. Pushover analysis was adopted here to further analyze the actual condition state of the church, in terms of damage distribution and its resistance to earthquakes. The damage distribution was assumed as given by the maximum principal strains as an indication of cracking. In order to validate the results in terms of base shear ratios, a load coefficient was defined as the ratio of the total horizontal and the total vertical loads of the structure.

Two different load patterns and different directions of the load application were taken into account due to the planar irregularity of the structure. As the structure is not symmetric, the seismic action shall be applied in both, positive and negative directions of loading directions. In the end, the obtained results were compared in terms of damage and load coefficient ratio with the results of similar collapse mechanisms obtained from the kinematic analyses. Finally, all the results were compared in order to determine the maximum seismic effects in the structure and the worst scenario for damage. Geometrical and physical non-linearity was considered in the analysis. The regular Newton-Raphson method, combined with the arc-length method, was adopted to obtain the solution of the non-linear problem arising from the equilibrium and compatibility conditions.

The non-linear behavior of the masonry was modeled by the adoption of a constitutive model based on total strain model, Diana (2009). This is an isotropic model with a compressive cap and fixed smeared cracking. This model was selected because it provides good stability in the opening crack control and moderate computer cost. It is noted that much more sophisticated material models are available in the literature, namely considering the orthotropic behavior of masonry, see Lourenço (2002) for a review. More complex material models require additional data, which is hardly available, and still fail to represent the multi-leaf nature of most historic masonry structures. The adopted model provides a good compromise between accuracy and simplicity. Exponential softening was adopted for tension whereas parabolic hardening, followed be parabolic and exponential softening, was adopted for compression. The post-cracked shear behavior was modeled using a shear retention factor of 0.05. In order to ensure mesh independency of the solution, the fracture energy was regularized taking into account the finite element size.

The relation $E = \alpha \cdot f_c$ between the Young's modulus E and the compressive strength f_c is rather variable for masonry, with values of α ranging between 200 and 1000 according to Tomazevic (1999), even if the proposed value in EN 1996-1-1 (2005) is 1000. For dry stone masonry, PIET-70 (1971) proposes a value of $\alpha = 500$, which is in the mid range of the interval of Tomazevic (1999) and was adopted here ($f_c = E/500$). The ductility index for the compressive fracture energy was assumed equal to 1.6 mm. The masonry tensile strength was assumed equal to 5% of the compressive strength and the tensile fracture energy was assumed equal to 50 N/m (Lourenço, 2009).

Figure 17 shows the results in terms of load-displacement diagrams along the global (X, Y) and principal (X',Y') directions. Highly non-linear behavior is exhibited by the structure, with some saw-tooth diagrams due to the combination of a relatively

coarse mesh and the successive opening of cracks with strong softening behavior. Full details of the analyses and a discussion of the successive cracks that appear in the structure are given in Trujillo (2009). As expected, the response is non-symmetric, with significantly different responses when the load is applied in the positive or negative direction of the axes. It also can be observed that the response in global and principal axes are similar, with the exception of –Y' which is considerably lower than –Y. The lowest value of the maximum load coefficient for all directions is about 0.10 and the difference between the X and Y directions in terms of lowest value of maximum load coefficient is rather small. Both observations are in good agreement with the results obtained for limit analysis, even if the severe simplifications in limit analysis are again stressed. Finally, it can be observed that the first mode proportional loading provides load coefficients much lower than the mass proportional loading pattern.

Figure 18 shows the collapse mechanisms found for uniform loading along the global axes, depicted using deformed meshes and damaged zones. It is clear that some damage patterns do not fully represent the hinge distribution assumed in the kinematic analysis of the selected collapse mechanism because the assumed collapse mechanism is a 2D simplified version of the real 3D mechanism, in which bending of the horizontal strip is present. Still, the failure mechanisms with the lowest load coefficients (+X and –Y), respectively Figure 18a and Figure 18d, are in very good agreement with the controlling failure modes obtained with limit analysis, respectively Figure 13 and Figure 11b. Note also that, differently from what is expected in an undamaged church and from what is observed when they are struck by earthquakes, the church collapses inwards and not outwards in the global X direction. The reasons are the lack of a roof or vaults present in the remainings and the presence of external buttresses, which increase the out-of-plane outwards capacity.

The collapse mechanisms for the principal axes (X′,Y′) are similar to the ones for the global axes (X,Y) and are not shown here, see Trujillo (2009) for details. Figure 19 shows the first mode proportional loading results, for the controlling failure mechanisms in each direction, where it is clear that the deformation is much more localized and the final damage pattern configurations represent slightly better the formation of the hinges assumed in the limit analysis.

Finally, it is noted that a non-linear time history (dynamic) analysis was also carried out. The definition of a collapse mechanism could not be found due to lack of convergence, possibly because the mechanisms in X and Y direction are competing, and because the model is too complex (note that different thicknesses are considered to represent existing damage and added masses are included). Still, convergence could be found up to earthquake records of 0.06g, with maximum displacements around 0.01 m in both directions, Trujillo (2009). A non-linear time history analysis considering the tensile strength with ideal plastic behavior was also carried out. Although unrealistic for masonry structures, this analysis had no convergence problems, which allowed to perform a qualitative analysis of the dynamic response, namely the development of the mechanisms. The damage configurations in the analysis are shown in Figure 20, where it is shown that the tower failure mechanism is triggered, whereas the north façade mechanism is not triggered. This further confirms the conclusions of the pushover analyses, which defined the tower as the weakest link. With respect to the macro-block limit analysis, the tower mechanisms and north façade mechanism have similar load coefficients. This is possibly due to the fact that the arching action was not considered in the north façade mechanism, which seems to provide too conservative results, unless the side connections are so deteriorated that no arching action is possible. The results seem comparable with the mass proportional loading pushover analysis in the Y

direction and in between the mass and first mode proportional loading pushover in the X direction. The seismic demand obtained is not comparable with the first mode proportional loading pushover. This confirms the results of Peña *et al.* (2010), which found unexpected low values when using first mode proportional loading in historic buildings.

The church of St. George of the Latins has features that make its dynamic behavior rather complex: (a) absence of in plan regularity; (b) absence of in elevation regularity; (c) distributed mass and stiffness; (d) low contribution of fundamental modes; (e) absence of rigid horizontal diaphragm. Although several authors have proposed new versions of pushover analyses, such as the multi-modal pushover introduced by Chopra and Goel (2002) applied to concrete structures, the application of this method of analysis to historical buildings is still a challenge and should be used with caution, as shown in Peña *et al.* (2010) for modal pushover, or Mendes and Lourenço (2010) for modal adaptative pushover,.

6 Conclusions

The results of an inspection and diagnosis campaign in one church remainings in Famagusta, Cyprus, were provided. The campaign includes visual inspection, sonic testing and dynamic identification. The church remainings require adequate conservation projects and their basis were established.

A detailed study of the stability of St. George of the Latins church under earthquake loading was carried out using different approaches. First, kinematic analysis of collapse mechanisms was applied. Then a non-linear static approach was used using a calibrated finite element models to perform classic pushover analyses. A non-linear

dynamic approach was also applied using advanced numerical modeling with time integration.

The following conclusions were possible: (a) Kinematic analysis of collapse mechanisms based on the damage patterns found in the visual inspection can be adequately used for masonry church remainings. The safety assessment by kinematic analysis of collapse mechanism provided a collapse for a horizontal acceleration equal or higher than 0.10g, with a similar vulnerability in both orthogonal directions; (b) The inclusion of damage patterns from visual inspection using a smaller thickness in elements located inside "damaged" regions was very useful to update the numerical model. The dynamic behavior of the structure is sensitive to the structural damage and rather low errors could be obtained in the frequencies estimation (average of 2%), with acceptable MAC values (average of 65%); (c) The safety of the structure assessed by performing pushover analyses with a horizontal load pattern proportional to the mass was only about 0.03g, which is not corroborated by a time history dynamic analysis. The safety of the structure assessed by performing pushover analyses with a mass horizontal load pattern was about 0.10g, which is similar to the value obtained from the safety assessment by limit analysis; (d) The seismic capacity was much lower than the recommended demand from the Cyprus national annex (CYS EN 1998-1:2004, 2007), which is about 0.35g, meaning that the church remainings are rather vulnerable to earthquake loading.

Acknowledgements

This work was partly funded by project FP7-ENV-2009-1-244123-NIKER of the 7th Framework Programme of the European Commission Project.

References

Binda, L, Saisi, A., Tiraboschi, C., Valle, S., Colla, C., Forde, M. (2003), Application of sonic and radar tests on the piers and walls of the Cathedral of Noto, Construction and Building Materials, 17(8), p. 613-627.

Chopra, A.K., Goel, R. K. (2002), A modal pushover analysis procedure for estimating seismic demands for buildings, Earthquake Engineering and Structural Dynamics, 31, p. 561–582.

CYS EN 1998-1:2004 (2007). National Annex to Eurocode 8: Design of structures for earthquake resistance – General rules, seismic actions and rules for buildings, CYS.

DIANA. (2009). DIsplacement method ANAlyser. CD-ROM , Release 9.4. Netherlands.

Douglas, B.M., Reid, W. H. (1982). Dynamic tests and system identification of bridges. Structural Division, ASCE , 108, 2295-2313.

EN 1996-1-1:2005 (2005). Eurocode 6: Design of masonry structures. General rules for reinforced and unreinforced masonry structures, CEN.

EN 1998-1:2004 (2004). Eurocode 8: Design of structures for earthquake resistance – General rules, seismic actions and rules for buildings, CEN.

Giuffrè, A. (1993), Safety and conservation of historical centers: The case of Ortigia. Bari: Laterza (in Italian).

Heyman, J. (1966), The stone skeleton, International Journal of Solids and Structures, 2(2), 270-279.

Learid, J.B. (1984), A report on the pulsed acoustic emission technique applied to masonry, Journal of Acoustic Emission, 3(4).

Lourenço, P.B. (2002), Computations of historical masonry constructions, Progress in Structural Engineering and Materials, 4(3), p. 301-319.

Lourenço, P.B., Ramos, L.F. (2008), Preliminary report on the inspection on three Famagusta churches, Report 08-DEC/E-11, University of Minho, Guimarães.

Lourenço, P.B. (2009), Recent advances in masonry structures: Micromodelling and homogenisation, em: Multiscale Modeling in Solid Mechanics: Computational

Approaches, Eds. U. Galvanetto, M.H. Ferri Aliabadi, Imperial College Press, p. 251-294.

Lourenço, P.B., Mendes, N., Ramos, L.F., Oliveira, D.V. (2011), On the analysis of masonry structures without box behavior, International Journal of Architectural Heritage, 5(4).

Mendes, N., Lourenço, P.B. (2010), Seismic assessment of masonry "Gaioleiros" buildings in Lisbon, Portugal, Journal of Earthquake Engineering, 14, p. 80-101.

Municipality of Famagusta. (2009), The history of Famagusta. Retrieved March 1, 2011, from http://www.famagusta.org.cy.

O.P.C.M. 3431. (2005). Technical code for the seismic design, assessment and retrofit of buildings (in Italian).

PCM-DPC-MiBAC M.-A.-D. (2006), Form for the survey of damage in cultural heritage - Churches (in Italian). Scheda per il relievo del danno ai beni culturali – Chiese.

Peeters, B. (2000), System identification and damage detection in civil engineering, PhD Thesis, Catholic University of Leuven, Belgium.

Peña, F., Lourenço, P.B., Mendes, N., Oliveira, D.V. (2010), Numerical models for the seismic assessment of an old masonry tower, Engineering Structures, 32(5), p. 1466-1478.

PIET-70 (1971), Masonry works. Prescriptions from Instituto Eduardo Torroja. Higher Council of Scientific Researches, CSIC, Madrid, 1971.

Ramos, L.F., Marques, L., Lourenço, P.B., De Roeck, G., Campos-Costa, A., Roque, J. (2010a), Monitoring of Historical Masonry Structures with Operational Modal Analysis: Two Case Studies, Mechanical Systems and Signal Processing, 24(5), p. 1291-1305.

Ramos, L.F., De Roeck, G., Lourenço, P.B., Campos-Costa, A. (2010b), Damage identification on arched masonry structures using ambient and random impact vibrations, Engineering Structures, 32(1), p. 146-162.

Tomazevic, M. (1999), Earthquake-resistant and design of masonry buildings, Imperial College Press, London.

Trujillo, A. (2009), Stability analysis of Famagusta churches: St. George of the Latins, MSc Thesis, University of Minho, Guimarães. Available from http://www.msc-sahc.org/

Unit of Environmental Studies. (2004). Cyprus geological heritage educational tool. (Research & Development Center - Intercollege). Retrieved March 1, 2011, from http://www.cyprusgeology.org/

Valluzzi, M. R., Cardani, G., Binda, L., Modena, C. (2004). Seismic vulnerability methods for masonry buildings in historical centres: Validation and application for prediction analyses and intervention proposals, 13th World Conference on Earthquake Engineering. Vancouver, Canada.

Vasconcelos, G., Lourenço, P.B., Alves, C.A.S., Pamplona, J. (2008), Ultrasonic evaluation of the physical and mechanical propertties of granites, Ultrasonics, 48, p. 453-466.

Walsh, M.J.K. (2007), Famagusta 2007: An appeal for international cooperation, in: ICOMOS World Report 2006/2007 on Monuments and Sites in Danger, Edited by Michael Petzet and John Ziesemer.

Walsh, M.J.K. (2010), "The Vile Embroidery of Ruin": Historic Famagusta between Ottoman and British Empires in *Fin de Siécle* Cyprus: 1878-1901, Journal of Intercultural Studies, 31(3), p. 247 – 269.

List of Figures

List of Tables

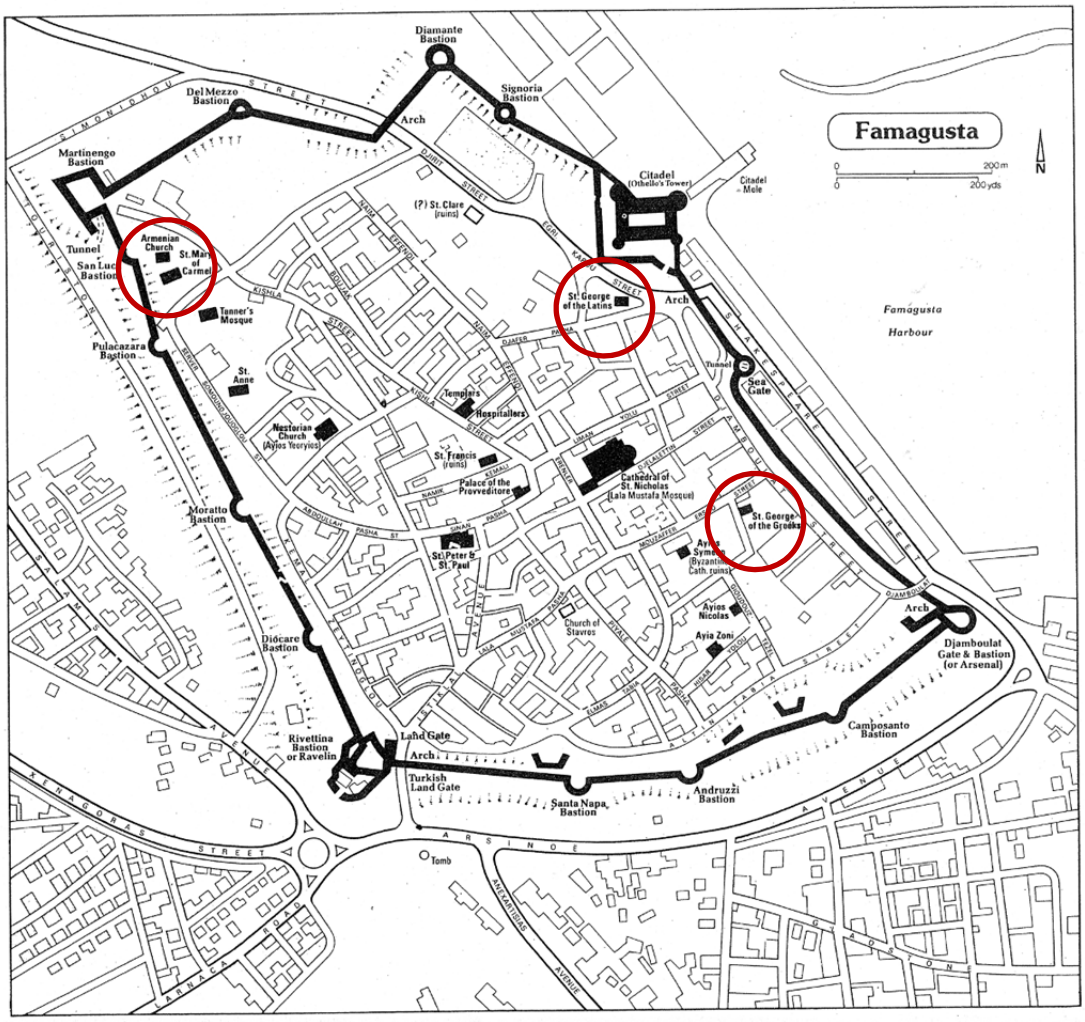

Figure 1 - Map of Famagusta walled city and location of the three churches selected.

(a)

(b)

Figure 2 – Historical photographs: (a) 1939-1941 situation vs. current condition;

(b) clear presence of new (lighter) stone.

(a)

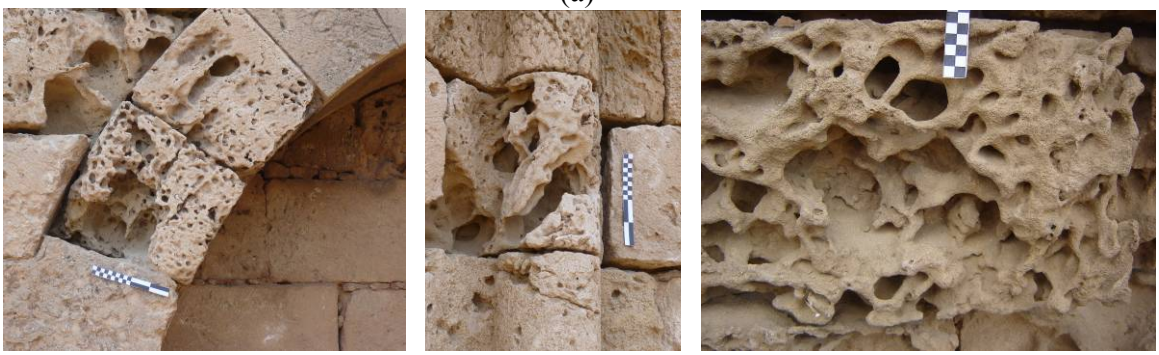

(b)

(c)

(d)

Figure 3 – Details on current condition: (a) the need keep to space clean and prevent misuse of room, currently used as toilet; (b) severe stone deterioration; (c) loose stone elements, which must be consolidated or removed; (d) highly corroded reinforced concrete lintel in main door.

(a)

(b)

Figure 4 – Details on current structural condition: (a) mostly inefficient buttresses due to stone deterioration; (b) a crack / rotation of the tower, possibly due to a previous earthquake / foundation problems.

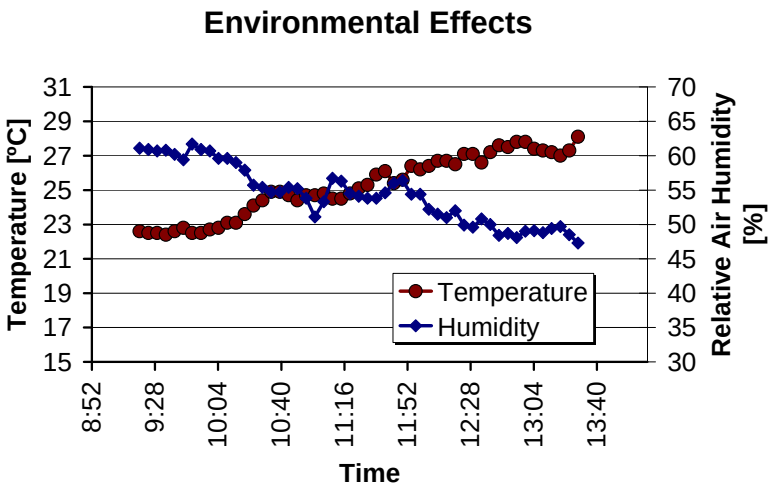

Figure 5 – Environmental effects recorded during modal identification tests in St. George of the Latins Church.

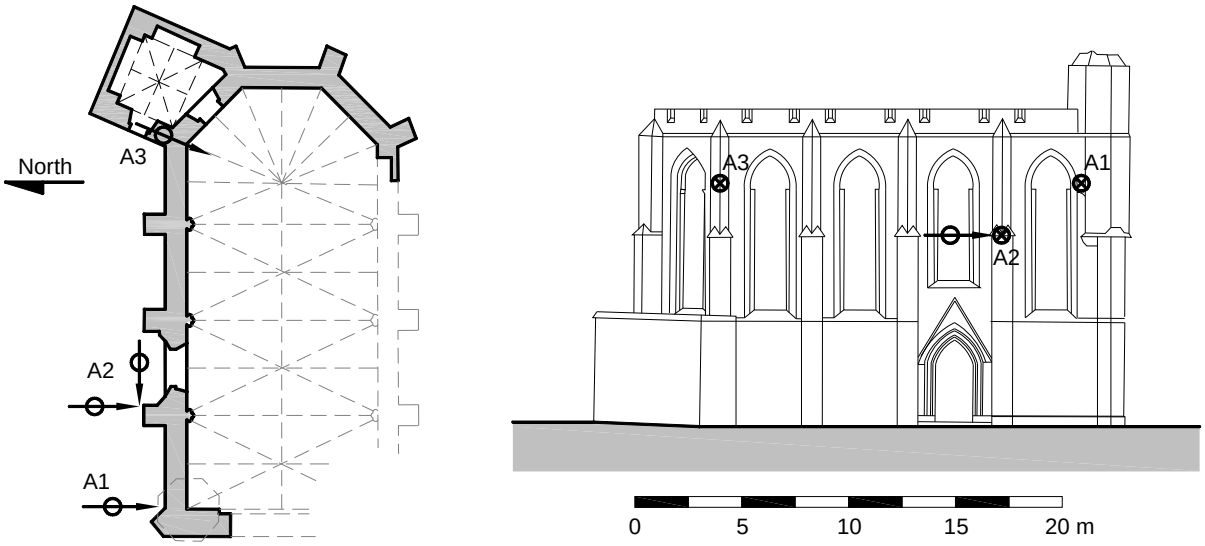

(a) (b)

Figure 6 – Test planning of St. George of the Latins church: (a) top plan; and (b) north façade.

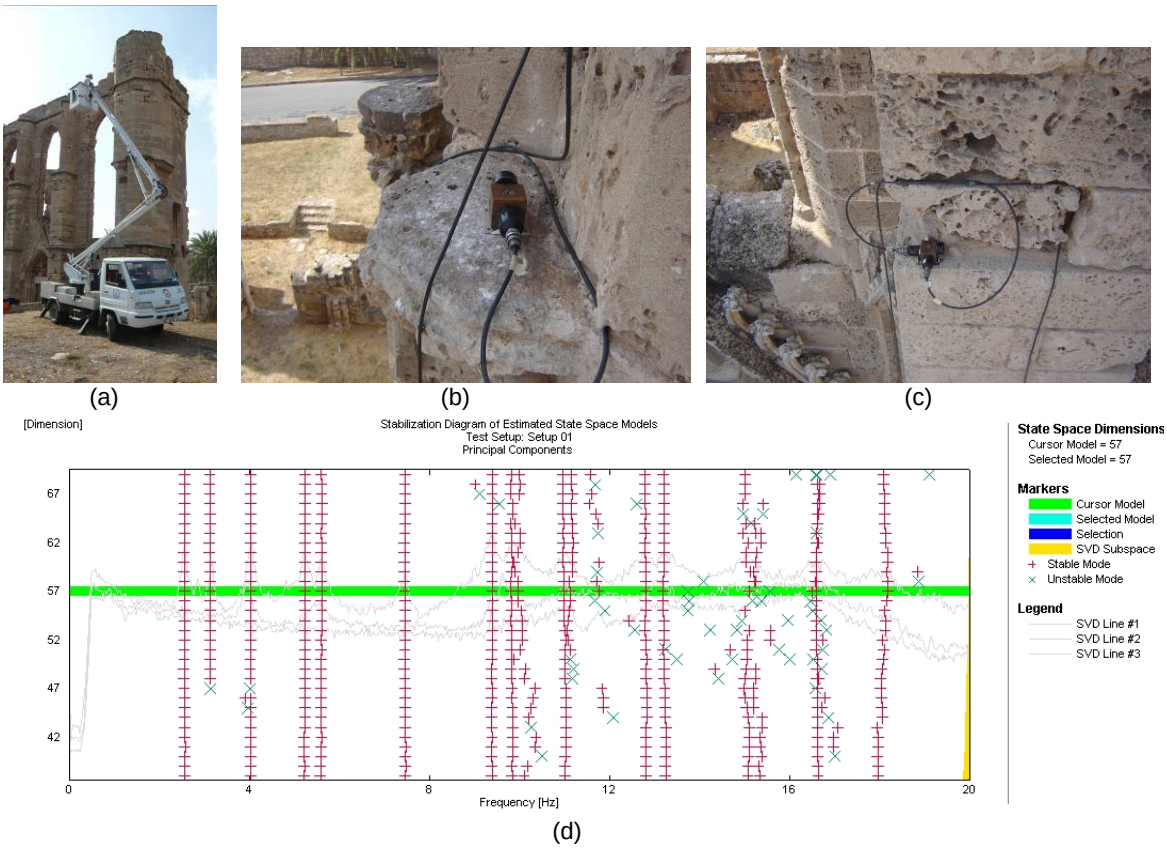

Figure 7 – Dynamic test at St. George of the Latins church: (a) lorry used to fix the sensors in the structure; (b) accelerometer at position A1; (c) accelerometers at position A2; and (d) stabilization diagram.

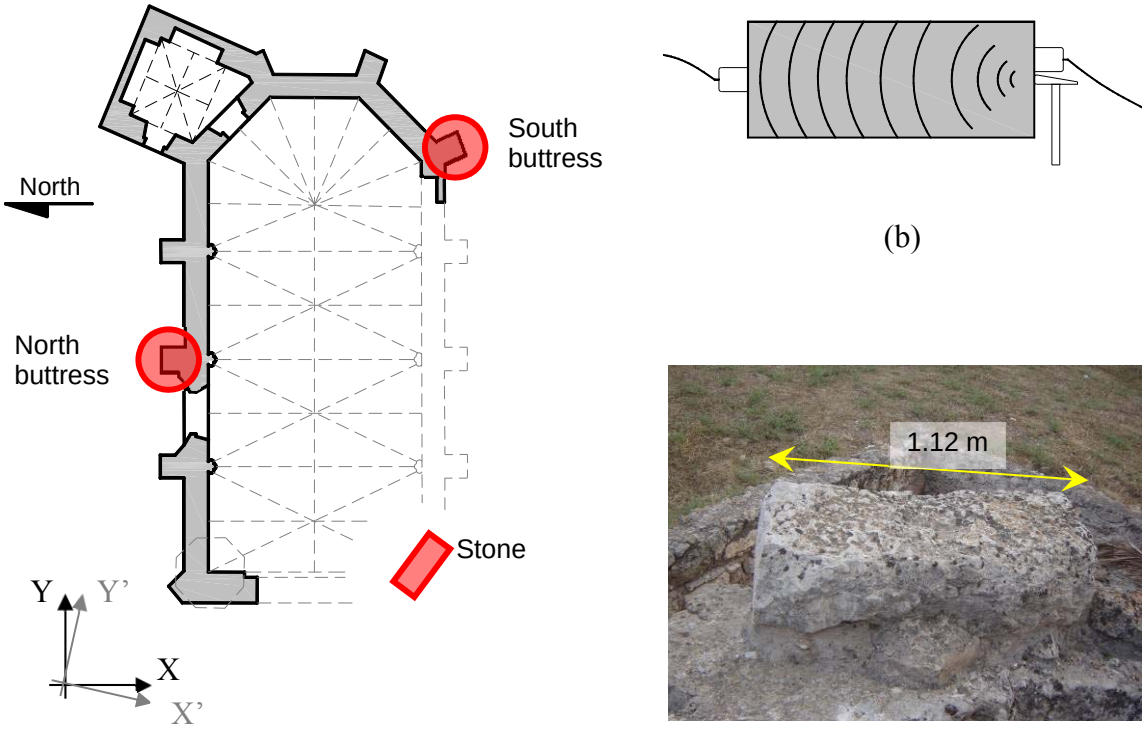

Figure 8 – Sonic tests in St. George of the Latins church: (a) selected buttresses and block stone; (b) test setup for the stone block; and (c) image of the stone block.

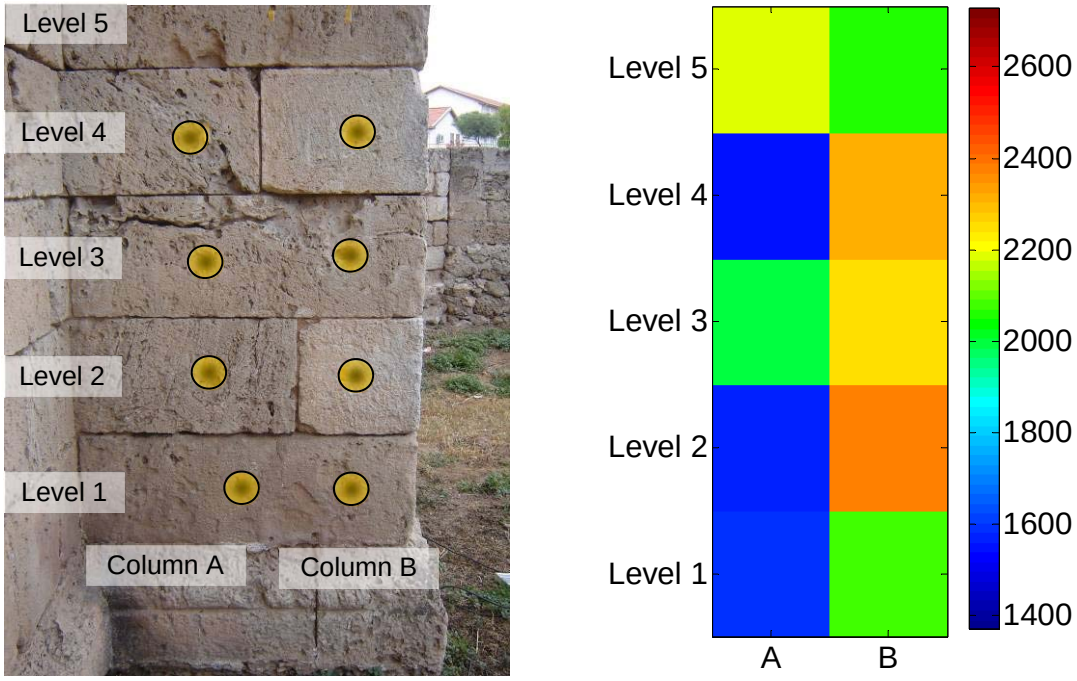

(a) (b)

Figure 9 – Sonic tests in the north buttress: (a) location of the measuring points; and (b) velocity map (m/s).

(a)

(b)

(c)

(d)

(e)

Figure 10 – West façade: (a) general view, (b) weak connection in upper part due to tower rotation, (c) severe deterioration of stones in the connection with north façade, (d) severe stone deterioration in lower part and (e) replaced (lighter) stones during conservation works in 1940.

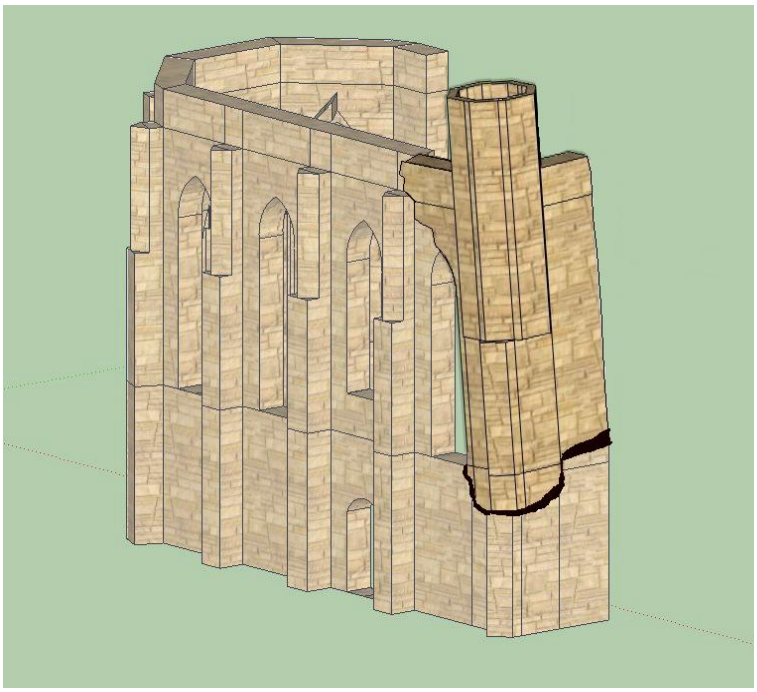

(a)

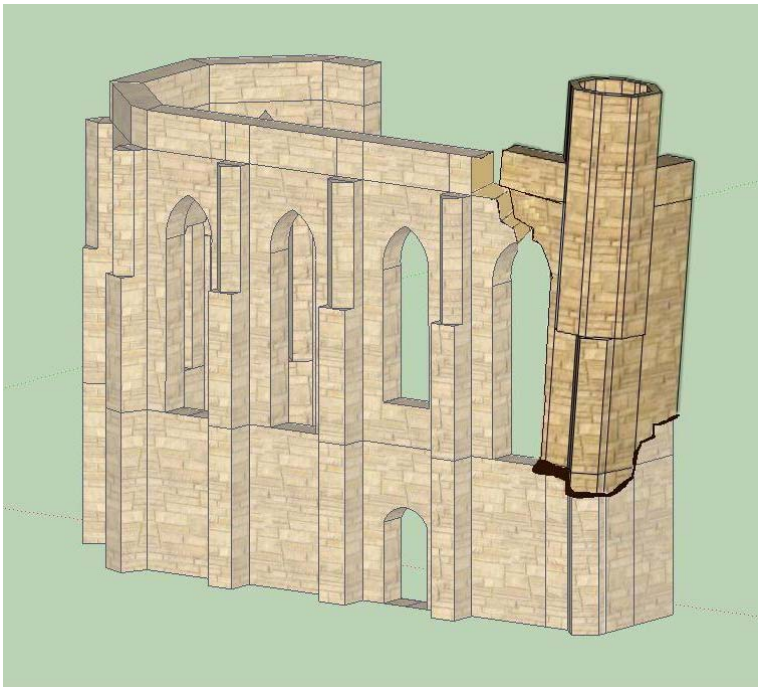

(b)

Figure 11 – Macro-elements defined for the West façade: (a) overturning for –X direction; overturning for –Y direction.

(a)

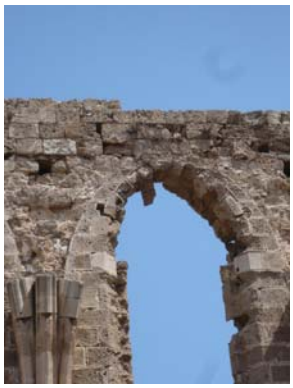

(b)

(c)

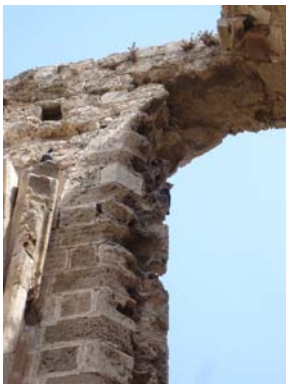

(d)

Figure 12 – North façade: (a) external view, (b) upper part of the second window; (c) crack opening and sliding in the connection with west façade; (d) crack opening and sliding in the connection with the apse.

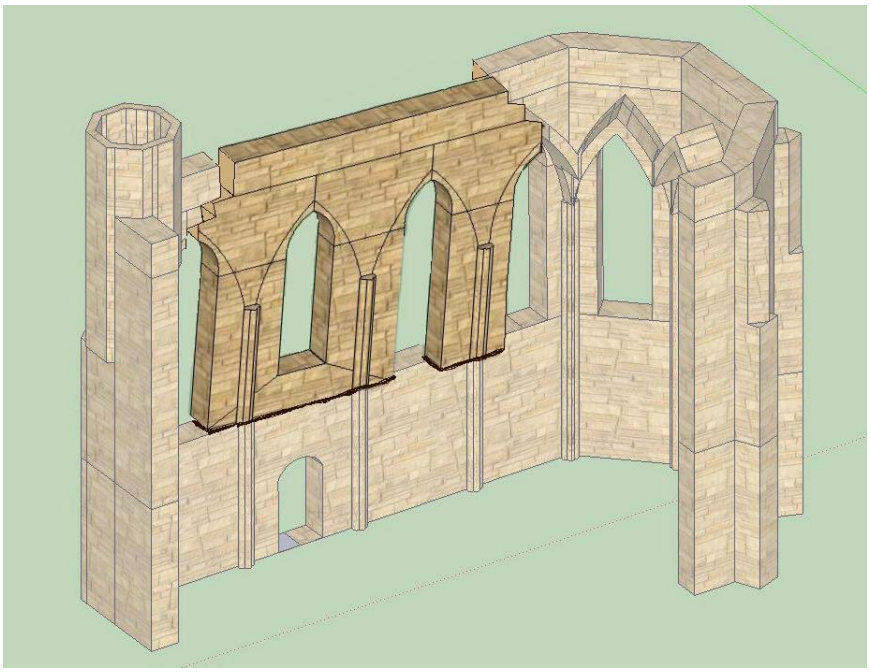

Figure 13 – Macro-element defined for the North façade: overturning for X direction.

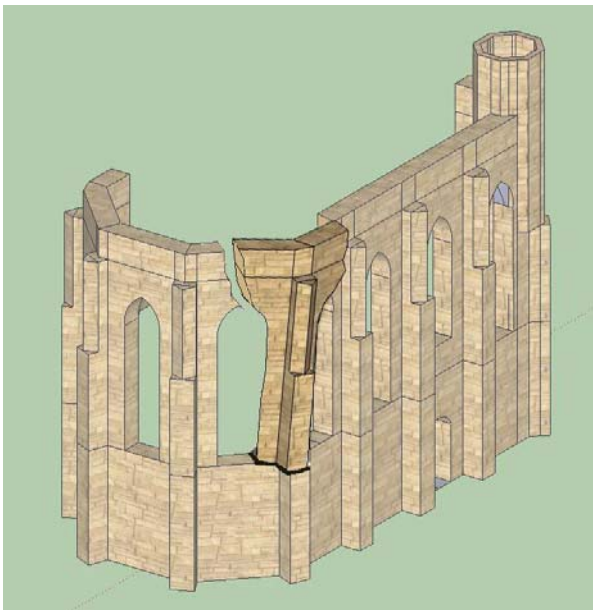

(a)

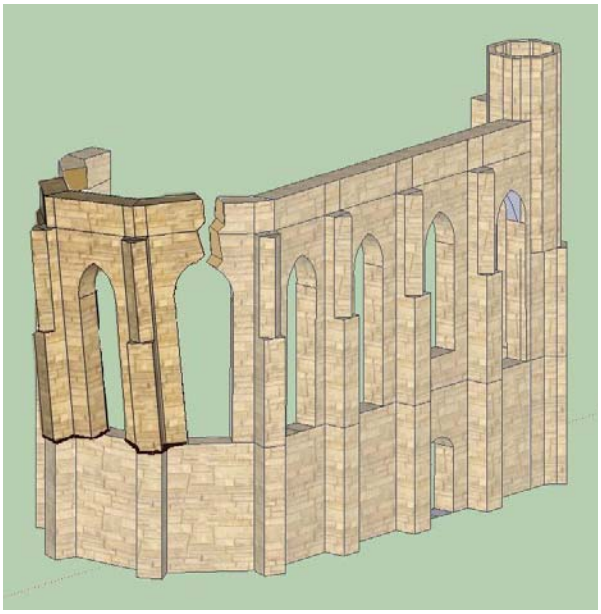

(a)

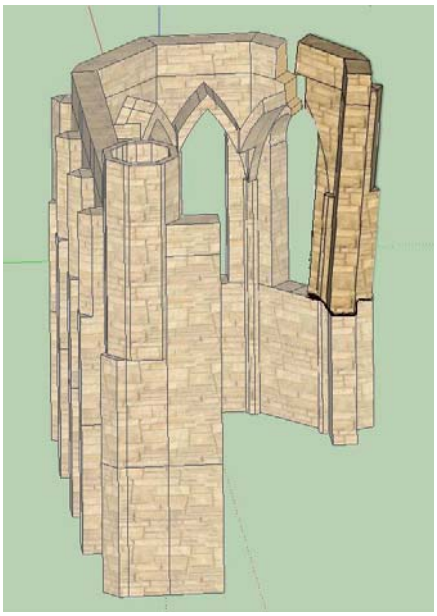

(c)

Figure 14 – Macro-elements defined for the apse: (a) overturning for X and X' direction; (b) overturning for Y direction; (c) overturning for X and X' direction.

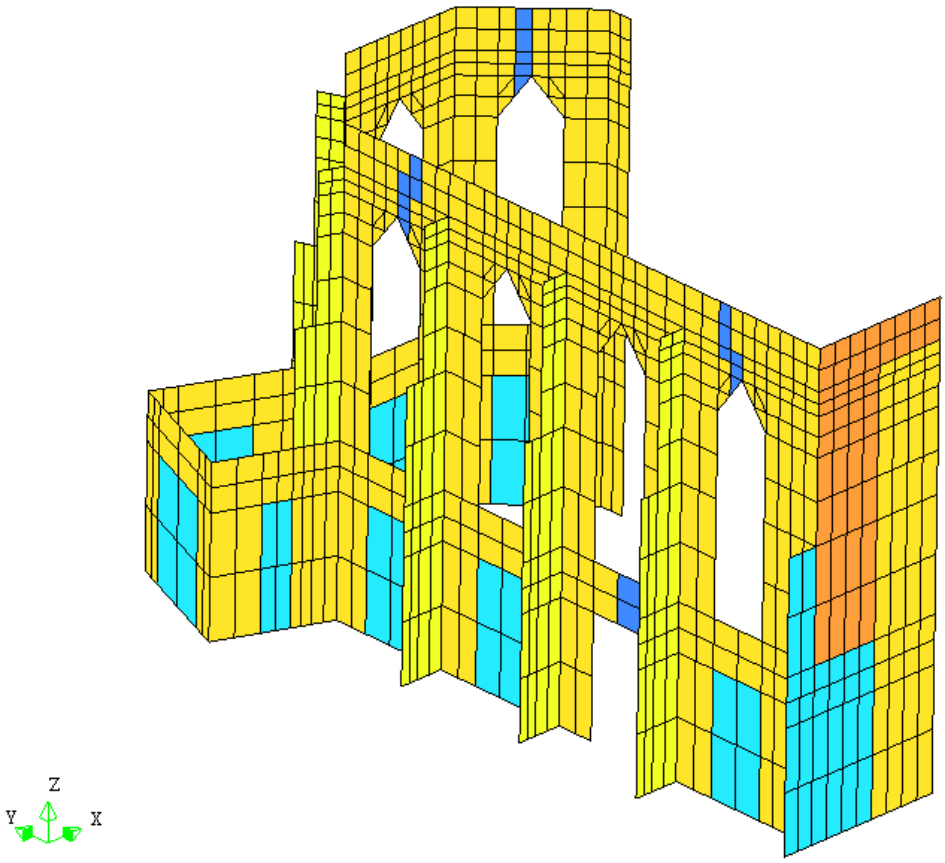

Figure 15 – Numerical model adopted for further updating based on dynamic identification (each shade indicates a different thickness).

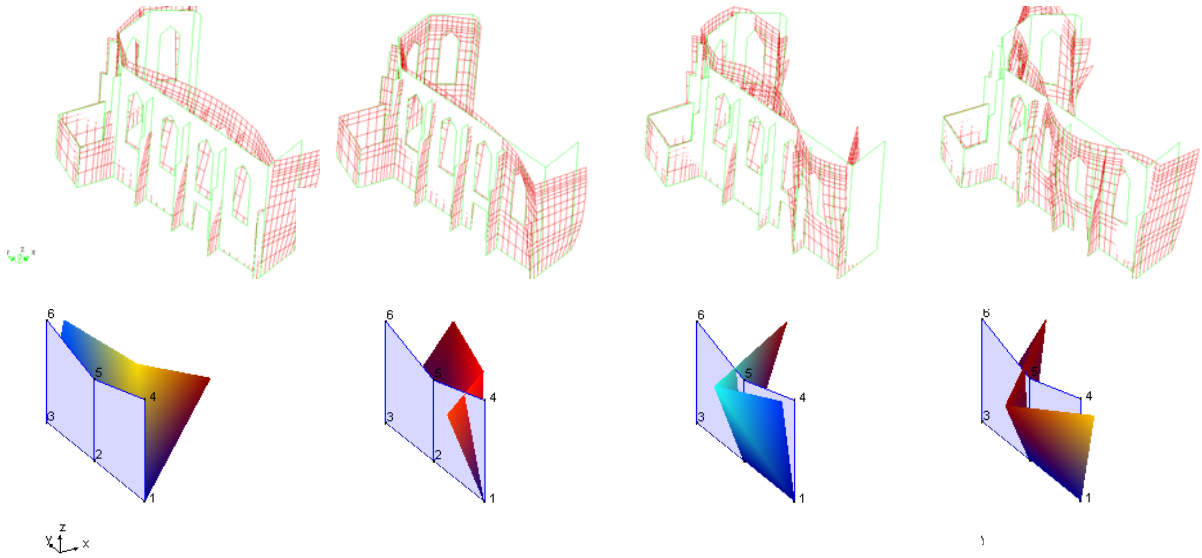

Figure 16 – Qualitative comparison between model and experimental mode shapes after calibration: (a) 1st mode; (b) 3rd mode; (c) 4th mode; (d) 6th mode.

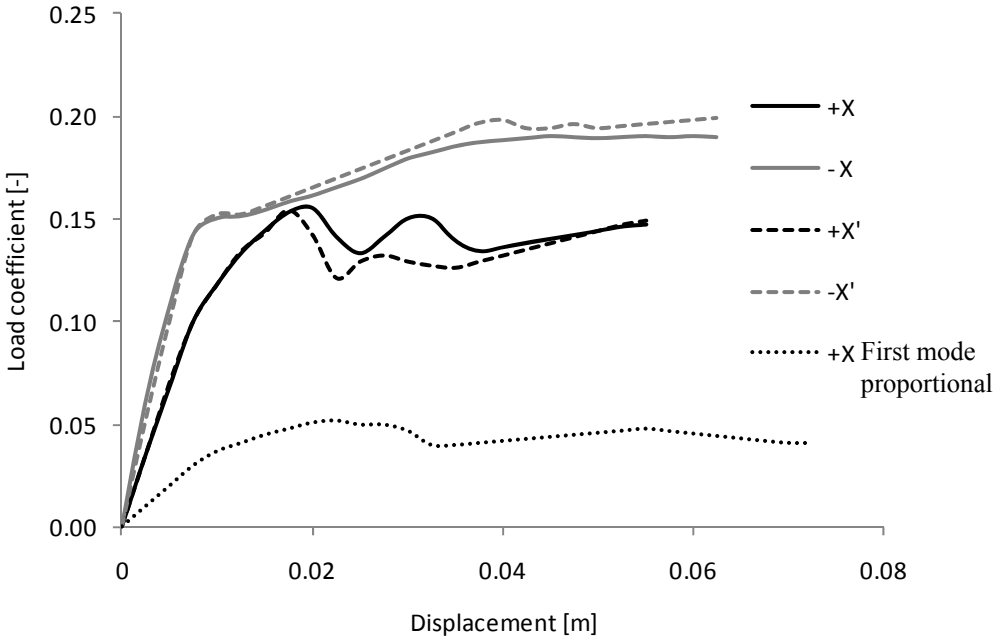

(a)

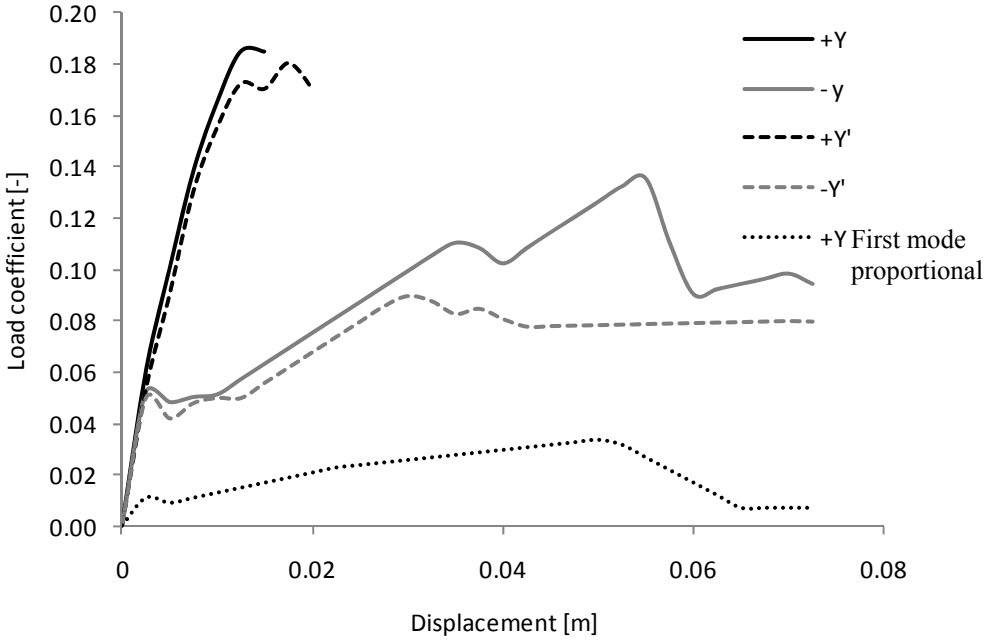

(b)

Figure 17 – Results from pushover analysis for mass proportional loading, except the ones with the suffix Mode: (a) transverse direction; (b) longitudinal direction.

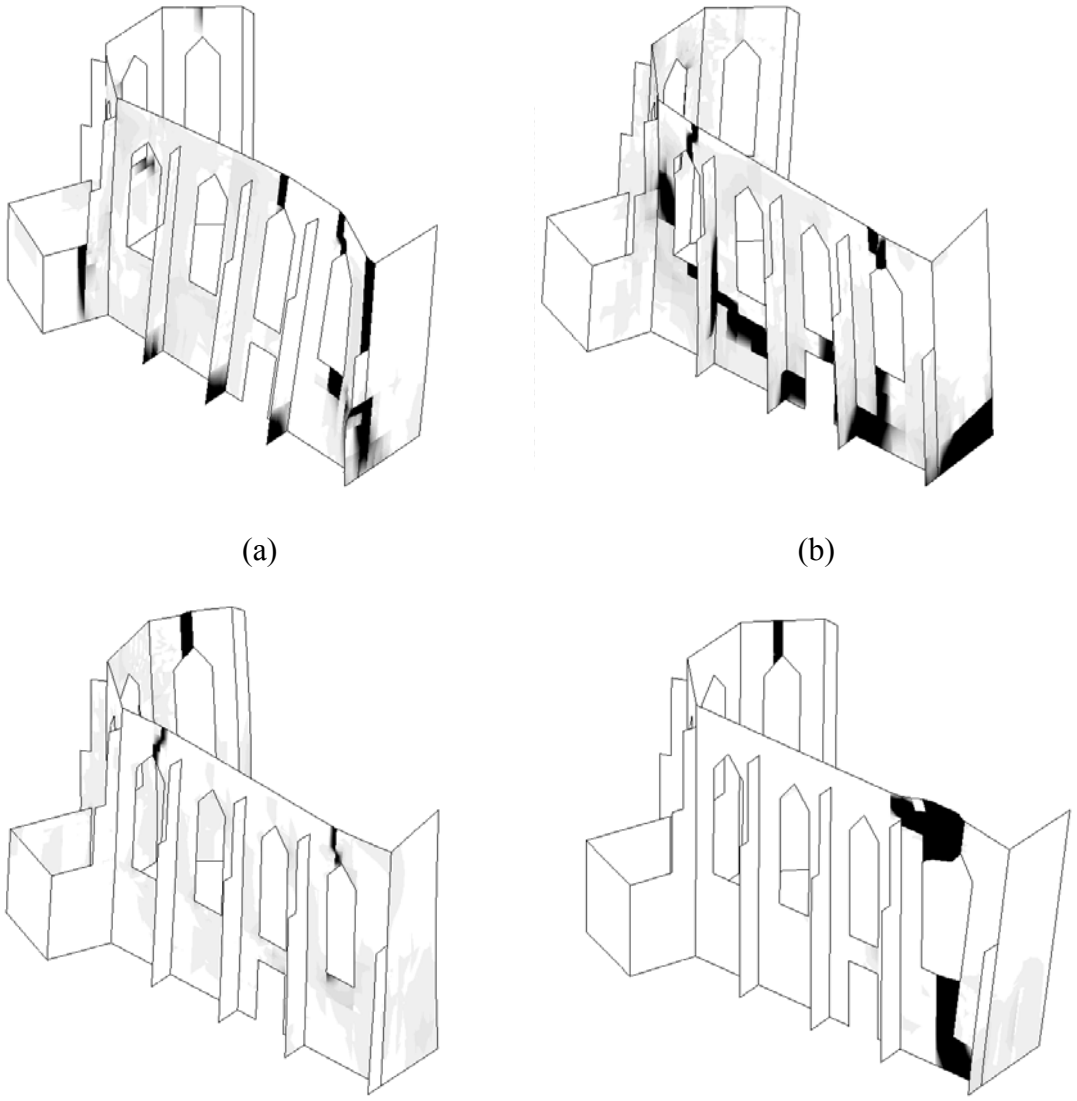

(a) (b)

(c) (d)

Figure 18 – Failure modes for mass proportional loading along global axis, with representation of maximum principal strains (as a measure of crack width): (a) +X; (b) –X; (c) +Y; (d) –Y.

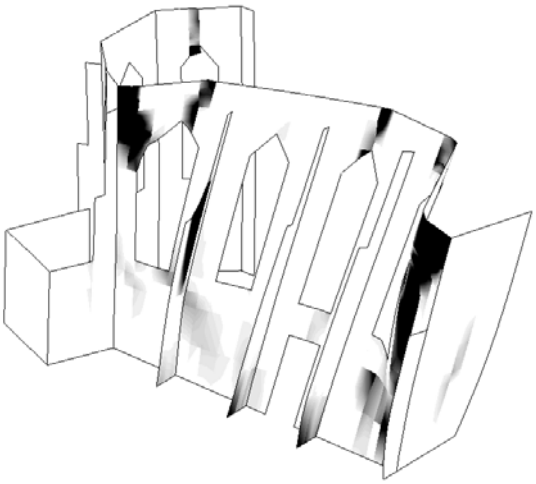

(a)

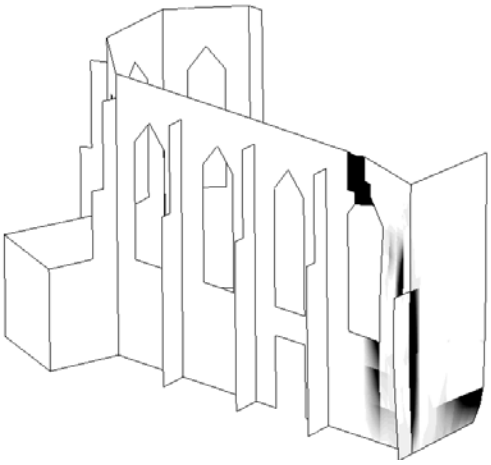

(b)

Figure 19 – Failure modes for first mode proportional loading along global axis, with representation of maximum principal strains (as a measure of crack width): (a) +X; (b) –Y.

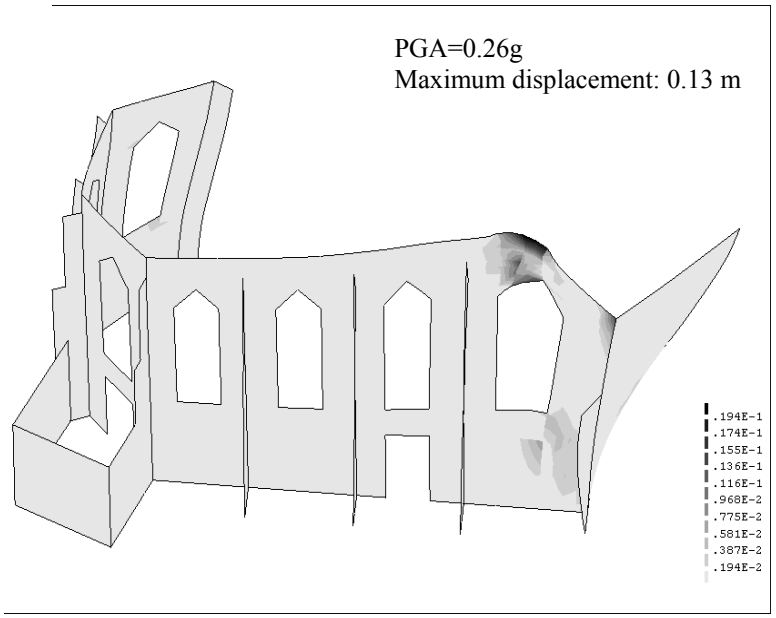

(a)

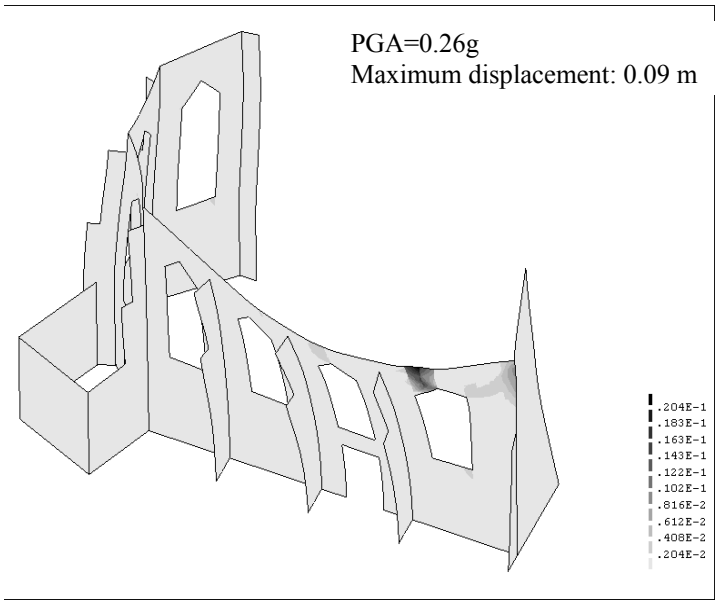

(b)

Figure 20 – Failure modes for non-linear dynamic history analysis, with representation of maximum principal strains (as a measure of crack width): (a) West façade overturning; (b) North façade overturning.

Table 1 – Results for the dynamic identification of St. George of the Latins church.

Mode	Frequency Values	Frequency Standard Deviation	Damping Values	Damping Standard Deviation	Description
	[Hz]	[Hz]	[%]	[%]	
1	2.57	<0.01	1.04	0.38	1st Out-of-plane bending
2	3.14	0.01	1.05	1.02	2nd Out-of-plane bending
3	3.95	0.06	0.55	0.57	3rd Out-of-plane bending
4	4.06	0.02	0.58	0.14	4th Out-of-plane bending
5	5.26	0.02	0.85	0.16	5th Out-of-plane bending
6	5.61	0.02	0.77	0.21	6th Out-of-plane bending

Table 2 – Results for the sonic velocities in the two buttress [m/s].

	North Buttress		South Buttress	
	Column A	Column B	Column A	Column B
Level 1	1316	2040	2259	1371
Level 2	1292	2498	2395	2730
Level 3	1911	2311	1888	2152
Level 4	1257	2385	1695	1647
Level 5	2211	2011	1377	2080
Average	1597	2249	1923	1996
Standard Deviation	437	215	415	520
CV	27%	10%	22%	26%

Table 3 – Results for load coefficient using limit analysis.

	West Façade X	West Façade Y	North Façade X	Apse X1	Apse Y'	Apse Y	Apse X2	Apse X'
Load factor	0.136	0.109	0.097	0.213	0.163	0.170	0.195	0.120

Table 4 – Material and physical properties after calibration process (* indicates a calibrated value).

Parameter	**Unit**	**Value**
Thickness of North façade	[m]	1.02
Thickness of damage (N-façade)	[m]	0.418*
Thickness of Apse & Sacristy	[m]	1.02
Thickness of damage (Apse)	[m]	0.100*
Thickness of West façade	[m]	1.29
Thickness of damage (W-façade)	[m]	0.340*
Thickness of Buttresses	[m]	0.95
Thickness of Top wall (North and Apse)	[m]	1.02
Thickness of Top wall (West)	[m]	1.29
Thickness of Blind arches walls	[m]	0.60
Thickness of Blind arch wall (West)	[m]	1.02
Unit weight of masonry	[kN/m³]	16
Elastic Modulus	[MPa]	3017*
Poisson's ratio	[-]	0.2
Additional mass of the tower	[kg]	52632
Additional mass of the vault	[kg]	32752

Table 5 – Comparison between experimental and numerical frequencies and mode shapes after calibration.

Mode Shape	f_{EXP} [Hz]	f_{NUM} [Hz]	Error [%]	MAC [%]	Mass part. in X [%]	Mass part. in Y [%]
1st	2.57	2.43	-5.45	94.2	32.49	0.01
3rd	3.14	3.19	1.59	49.8	5.47	12.34
4th	3.95	3.95	0.00	40.8	1.21	7.83
6th	5.26	5.29	0.57	76.5	2.96	3.41